JACS
JOURNAL OF THE AMERICAN CHEMICAL SOCIETY

ARTICLE

pubs.acs.org/JACS

Phase Selection and Site-Selective Distribution by Tin and Sulfur in Supertetrahedral Zinc Gallium Selenides

Tao Wu,[†] Xianhui Bu,[‡] Xiang Zhao,[†] Ripsime Khazhakyan,[†] and Pingyun Feng*[,†]

[†]Department of Chemistry, University of California, Riverside, California 92521, United States

[‡]Department of Chemistry and Biochemistry, California State University, 1250 Bellflower Boulevard, Long Beach, California 90840, United States

Supporting Information

ABSTRACT: Doping is among the most important methods to tune the properties of semiconductors. For dense phase semiconductors, the distribution of dopant atoms in crystal lattices is often random. However, when the size of semiconductors becomes increasingly smaller and reaches the extreme situation as is the case in chalcogenide supertetrahedral clusters, different chemically distinct sites (e.g., corner, edge, face, and core) occur, which can dramatically affect the doping chemistry at different sites and also spatial assembly of such clusters into covalent superlattices. In this work, we use the Zn−Ga−Se supertetrahedral clusters and their frameworks as the model system to examine the doping chemistry of Sn^{4+} and S^{2-} in the Zn−Ga−Se clusters. A series of selenide clusters (undoped supertetrahedral T4-ZnGaSe, S-doped T4-ZnGaSeS, Sn-doped T4-ZnGaSnSe, and dual S- and Sn-doped T4-ZnGaSnSeS) have been prepared with various levels of Sn- and S-doping and with different superlattice structures (OCF-1, -5, -40, and -42). The complex compositional and structural features of these materials are dictated by the convoluted interplay of three key factors: (1) the overall charge density and size/shape matching between clusters/frameworks and protonated guest amines determine the framework topology and the doping levels of Sn^{4+} and S^{2-}; (2) the site selectivity of Sn^{4+} is dictated by the local charge balance surrounding anionic Se/S sites as required by the electrostatic valence sum rule; and (3) the site selectivity and doping levels of sulfur is dictated by the location and amount of Sn based on hard soft acid base (HSAB) principle. The cooperative effect of amine-templating and doping by Sn and/or S leads to a rich chemical system with tunable framework compositions, topologies, and electronic properties.

1. INTRODUCTION

For several decades, solid-state chalcogenide semiconducting materials have been extensively studied owing to their wide applications in thermoelectrics, photoelectrics, and photocatalysis.[1−3] Recently, research on crystalline porous chalcogenides with various structural topologies and compositions has attracted increasing attention because these materials integrate open-framework architecture with semiconducting properties, and their high surface area and size/shape selectivity could contribute to improved device efficiency and may also help to generate new applications.[4]

For both dense or porous semicondutors, great efforts have been made to tune their band structures. In this aspect, designing materials with new compositions (or structures) and tuning properties of known materials represent two potent ways to create materials with desirable electronic structures. Toward this goal, we and others have studied a variety of self-assembly processes involving mono- or divalent transition metal ions (such as Cu^{+}, Zn^{2+}), high-valent main group metal ions (such as Ga^{3+}, In^{3+}, Ge^{4+}, Sn^{4+}), and chalcogenide anions (S^{2-}, Se^{2-}, Te^{2-}).[5−13] Many of the resulting open-framework covalent superlattices are built up from corner-sharing supertetrahedral clusters (denoted as Tn clusters, where n is the number of metal sites on each edge of the cluster).[11h] These previous studies on supertetrahedral clusters were mostly focused on the metal sulfide composition. In comparison with sulfides, the metal selenide Tn clusters have received less attention or their synthesis has been far less successful.[12]

The use of doping to tune electronic structures is a well-established method that has been successfully used for many years, usually for dense phase solid materials.[14−16] In general, the distribution of metal and nonmetal dopants in the crystal lattice is random. As the trend toward the use of semiconductor nanoparticles accelerates and as the applications of porous materials become more widespread, chalcogenide clusters and open frameworks have become the focus of studies by many researchers.[8−13] In addition to chemical compositions, these

Received: April 6, 2011
Published: May 19, 2011

dx.doi.org/10.1021/ja203143q | J. Am. Chem. Soc. 2011, 133, 9616–9625

Table 1. Summary of Crystal Data and Refinement Results

name[a]	framework composition[b]	S. G.	*a* (Å)	*c* (Å)	*R*(*F*)
OCF-1-ZnGaSeS-TMDP	$[Zn_4Ga_{16}Se_{33-x}S_x]$	*I*-42*d*	42.093(6)	16.690(3)	9.09
OCF-5-ZnGaSe-AEP	$[Zn_4Ga_{16}Se_{33}]$	$I4_1/acd$	23.5937(8)	42.620(3)	6.03
OCF-5-ZnGaSnSe-AEP	$[Zn_4Ga_{13.58}Sn_{2.42}Se_{33}]$	$I4_1/acd$	23.0701(4)	41.4975(13)	5.94
OCF-5-ZnGaSnSe-ECHA	$[Zn_4Ga_{16-x}Sn_xSe_{33}]$	$I4_1/acd$	24.0985(4)	42.1852(6)	/
OCF-5-ZnGaSnSe-PZ	$[Zn_4Ga_{16-x}Sn_xSe_{33}]$	$I4_1/acd$	24.1267(3)	42.2013(8)	/
OCF-5-ZnGaSnSe-MP	$[Zn_4Ga_{16-x}Sn_xSe_{33}]$	$I4_1/acd$	24.0745(2)	42.1653(5)	/
OCF-5-ZnGaSnSe-DMMP	$[Zn_4Ga_{16-x}Sn_xSe_{33}]$	$I4_1/acd$	24.1324(6)	42.1976(4)	/
OCF-5-ZnGaSnSe-TMPR	$[Zn_4Ga_{16-x}Sn_xSe_{33}]$	$I4_1/acd$	24.1687(3)	42.2724(3)	/
OCF-5-ZnGaSeS-AEP	$[Zn_4Ga_{16}Se_{16.89}S_{16.11}]$	$I4_1/acd$	22.8934(12)	41.516(4)	7.04
OCF-5-ZnGaSeS-DPM	$[Zn_4Ga_{16}Se_{20.67}S_{12.33}]$	$I4_1/acd$	23.5451(2)	41.2267(8)	5.92
OCF-5-ZnGaSnSeS-TMDP	$[Zn_4Ga_{12.93}Sn_{3.07}Se_{28.13}S_{5.01}]$	$I4_1/acd$	24.1157(2)	41.9575(6)	6.80
OCF-5-ZnGaSnSeS-DAMP	$[Zn_4Ga_{13.87}Sn_{2.13}Se_{27.67}S_{5.39}]$	$I4_1/acd$	23.7021(3)	42.1858(8)	7.44
OCF-5-ZnGaSnSeS-ECHA	$[Zn_4Ga_{13.06}Sn_{2.94}Se_{29.70}S_{3.30}]$	$I4_1/acd$	23.6724(2)	42.2660(8)	7.07
OCF-5-ZnGaSnSeS-PR	$[Zn_4Ga_{14.17}Sn_{1.83}Se_{27.57}S_{5.52}]$	$I4_1/acd$	23.5849(3)	41.8710(17)	6.39
OCF-40-ZnGaSnSeS-PR	$[Zn_4Ga_{14}Sn_2Se_{31.71}S_{3.29}]$	*I*-43*m*	18.7047(10)	18.7047(10)	3.45

[a] TMDP = 4, 4′-trimethylenedipiperdine, $C_{13}H_{26}N_2$; AEP = *N*-(2-aminoethyl)piperazine; PR = piperidine, $C_5H_{11}N$; ECHA = *N*-ethylcyclohexanamine, $C_8H_{12}N$; PZ = piperazine, $C_4H_{10}N_2$; DPM = dipiperidinomethane, $C_{11}H_{22}N_2$; DAMP = 1,5-diamino-2-methylpentane, $C_6H_{16}N_2$; MP = morpholine, C_4H_9NO; DMMP = 2,6-dimethylmorpholine, $C_6H_{13}NO$; TMPR = 2,2,6,6-tetramethylpiperidine, $C_9H_{19}N$. [b] The elemental composition ratio in some selected good crystals is determined by structural refinement.

cluster-based open framework materials provide an additional level of control over the electronic properties through their varying degree of porosity and patterns of spatial assemblies between clusters. To further control the electronic properties of these materials, it is useful to also study the doping chemistry in these cluster-based open framework materials.

In this work, we aim to study how the compositions, structures, and electronic properties can be controlled by the combined amine-templating and doping by Sn or S in the Zn−Ga−Se system. The selection of Sn(IV) and S has distinct advantages in providing tunable framework charge density because Sn(IV) decreases the overall negative charge of the cluster and increase the cluster size, while S decreases the cluster size. Furthermore, because Sn-doping into Ga site generally causes a red shift while S-doping into Se sites causes a blue shift, this doping strategy allows a large range of band gaps to be achieved. By changing the amine type and doping strategy (no doping, Sn-doping only, S-doping only, and dual Sn- and S-doping), we have investigated a large number of synthetic systems (for each amine type, there are four different doping permutations). Here, we report a series of selenide compounds composed of T4 clusters and amine templates. These compounds are collectively named as OCF-*n*-composition-template (OCF = organically directed-chalcogenide frameworks, and *n* designates a specific framework topology, Table 1). Multicomponent supertetrahedral T4 clusters, such as ternary (T4-ZnGaSe), quaternary (T4-ZnGaSeS and T4-ZnGaSnSe), and pentanary (T4-ZnGaSnSeS), have been systematically synthesized and their optical properties investigated. Of particular interest are (1) the subtle control of different framework topologies via host−guest interactions tunable through Sn- and S-doping, (2) different Sn- and S-doping levels at different crystallographic sites and in materials with different topologies, (3) site selective distribution of metal ions and nonmetal ions, and (4) effects of these tunable compositional and structural features on the electronic properties.

2. EXPERIMENTAL SECTION

2.1. Materials and General Methods. All chemicals and solvents were of reagent grade and were used as purchased without further purification. Solid-state diffuse reflectance spectra were recorded on a SHIMADZU UV-3101PC UV−vis-NIR Scanning Spectrophotometer by using $BaSO_4$ powder as 100% reflectance reference. Powder X-ray diffraction data were collected using a Bruker D8-Advance powder diffractometer operating at 40 kV, 40 mA with Cu Kα (λ = 1.5406 Å) radiation (2θ range, 2−40°; step size, 0.03°; scan speed, 60 s/step). Semiquantitative elemental analyses were performed with a Philips FEI XL30 scanning electron microscope (SEM) equipped with energy dispersive spectroscopy (EDS) detector.

2.2. Synthesis. The sulfur source and tin source used in this paper are dimethyl sulfoxide (DMSO) and anhydrous tin(II) chloride, respectively. All reactions were carried out at 200 °C.

2.2.1. Typical Synthesis of Quaternary Sulfur-Doped OCF-1-ZnGaSeS-TMDP. $Ga(NO_3)_3 \cdot xH_2O$ (255.7 mg, ∼1.0 mmol), $Zn(NO_3)_3 \cdot 6H_2O$ (75.0 mg, 0.25 mmol), Se (177 mg, 2.24 mmol), and TMDP (4, 4′-trimethylenedipiperidine, 2.0 g, 9.51 mmol) were mixed with H_2O (3.0 g, 166.7 mmol) and dimethylsulfoxide (DMSO, 2.0 g, 25.60 mmol) in 23-mL Teflon-lined stainless steel autoclave and stirred for half an hour. The vessel was then sealed and heat up to 200 °C for 9 days. After cooling to room temperature, a large amount of pale-yellow octahedral crystals were obtained. These raw products were then washed by water and ethanol, and dried in air for other measurement. Yield: 121.2 mg.

2.2.2. Typical Synthesis of Tertiary Undoped OCF-5-ZnGaSe-AEP. $Ga(NO_3)_3 \cdot xH_2O$ (255.7 mg, ∼1.0 mmol), $Zn(NO_3)_3 \cdot 6H_2O$ (75.0 mg, 0.25 mmol), Se (177 mg, 2.24 mmol), and AEP (*N*-(2-aminoethyl)piperazine, 2.5 g, 19.35 mmol) were mixed with H_2O (3.0 g, 166.7 mmol) in 23-mL Teflon-lined stainless steel autoclave and stirred for 1 h. The vessel was then sealed and heat up to 200 °C for 9 days. After cooling to room temperature, a large amount of pale-yellow octahedral crystals were obtained. These raw products were then washed by water and ethanol, and dried in air for other measurement. Yield: 165.3 mg.

2.2.3. Typical Synthesis of Quaternary Tin-Doped OCF-5-ZnGaSnSe-ECHA. This compound was prepared in a synthetic procedure similar to

dx.doi.org/10.1021/ja203143q | J. Am. Chem. Soc. 2011, 133, 9616–9625

that for OCF-5-ZnGaSe-AEP, with the following two differences: (1) adding $SnCl_2$ (50.0 mg, 0.264 mmol) into the mixture and (2) replacing AEP with ECHA (*N*-ethylcyclohexanamine, 2.5 g, 19.64 mmol). Yield: 119.6 mg.

2.2.4. Typical Synthesis of Quaternary Sulfur-Doped OCF-5-ZnGaSeS-AEP. This compound was prepared in a synthetic procedure similar to that for OCF-5-ZnGaSe-AEP, except that DMSO (2.0 g, 25.60 mmol) was added into the mixture. Yield: 135.6 mg.

2.2.5. Typical Synthesis of Pentanary Tin- And Sulfur-Doped OCF-5-ZnGaSnSeS-TMDP. This compound was prepared in a synthetic procedure similar to that for OCF-1-ZnGaSeS-TMDP, except that $SnCl_2$ (50.0 mg, 0.246 mmol) was added into the mixture. Yield: 105.8 mg.

2.2.6. Typical Synthesis of Pentanary Tin- And Sulfur-Doped OCF-40-ZnGaSnSeS-PR. This compound was prepared in a synthetic procedure similar to that for OCF-5-ZnGaSnSeS-TMDP, with the following two differences: (1) replacing TMDP with piperidine (PR, 2.5 g, 29.36 mmol) and (2) decreasing the amount of DMSO to 1.0 g. Yield: 128.9 mg.

2.3. Single Crystal X-ray Crystallography Studies. Single-crystal X-ray analysis was performed on a Bruker Smart APEX II CCD area diffractometer with nitrogen-flow temperature controller using graphite-monochromated Mo Kα radiation (λ = 0.71073 Å), operating in the ω and φ scan mode with a scan width of 0.5°. Raw data collection was done at 150K. Data reduction was performed using SAINT$^+$. The SADABS program was used for absorption correction. The structure was solved by direct methods and the structure refinements were based on $|F^2|$. All non-hydrogen atoms were refined with anisotropic displacement parameters. Extra-framework organic amine molecules in OCF-1 and OCF-5 series of structures cannot be located owing to their disorder, which is the case in nearly all 3-D structures constructed from chalcogenide clusters. For molecular OCF-40, amine molecules are ordered and hydrogen atoms were placed in calculated positions. All crystallographic calculations were conducted with the SHELXTL software suites. Three constraint instructions (EXYZ, EADP, and SUMP) were used to refine relative occupancy factors of the mixed Sn/Ga sites and mixed Se/S sites.

Chemical compositions are determined by crystallographic refinements and are further confirmed by EDAX (Figure S1) and their phase purity is supported by powder X-ray diffraction (PXRD) (Figure S2).

3. RESULTS AND DISCUSSION

3.1. Determination and Selection of Optimum Synthesis Parameters. The large difference in the scattering factors between Se and S (and between Ga and Sn) makes it possible to determine the site-selective distribution of Se/S and Ga/Sn among different sites in the T4 cluster. However, the low crystal quality often exhibited by crystals containing large clusters can compromise the accuracy of the crystallographic results. To ensure the reliability in the determination of occupancy factors of Se/S and Ga/Sn, the quality of crystal data is essential. For this reason, a large number of synthetic trials were performed to identify the synthetic conditions for growing high quality crystals. All the data used for occupancy refinement reported here are based on the high quality diffraction data.

Although both Sn element and anhydrous tin(II) chloride allow the introduction of tin(IV) (through oxidation by Se) into Zn−Ga−Se compounds, tin(II) chloride is the preferred tin source, because metal tin usually gives poor-quality crystals, contaminated with inseparable impurities. Sulfur element was initially used as the sulfur doping reagent. While the doping of sulfur in T4 cluster was confirmed by the energy dispersive X-ray (EDAX) spectroscopy, poor crystal quality prevents the precise determination of the site distribution within the crystal. Dimethyl sulfoxide (DMSO) was later proved to be a good sulfur doping source for preparing sulfur-doped metal selenides with good crystal quality. In addition to DMSO, a number of other sulfoxide and thiourea reagents (Scheme 1) were also investigated as the sulfur source, but none forms crystals of sufficient quality for occupancy refinements.

Obviously, the doping level of sulfur in metal selenides can be tuned by adjusting the amount of DMSO. A low amount of DMSO may cause the coexistence of undoped T4-ZnGaSe and

Scheme 1. The Structure of Thiourea and Sulfone Molecules with Different Substituent Groups Used As Sulfur Sources

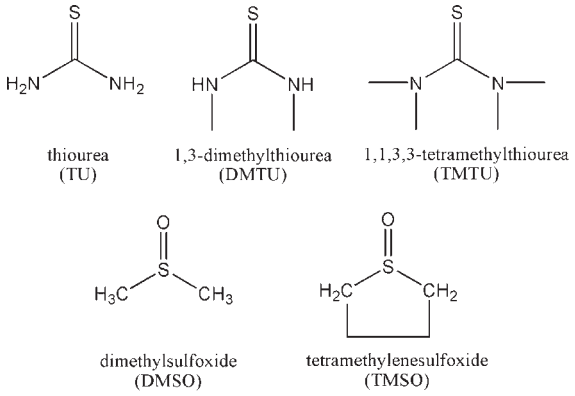

Scheme 2. The Name (Including Abbreviation) and Structure of Amine Template Molecules

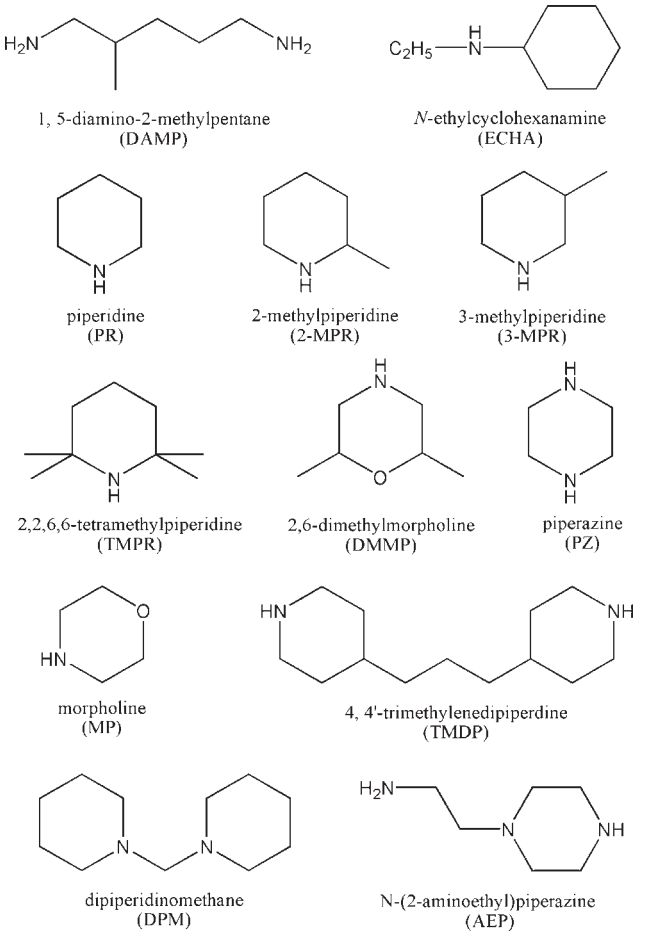

dx.doi.org/10.1021/ja203143q |*J. Am. Chem. Soc.* 2011, 133, 9616–9625

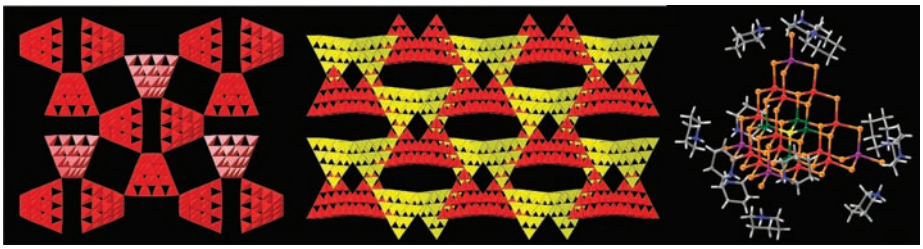

Figure 1. The structures of OCF-1, OCF-5, and OCF-40. The disordered amine template molecules in OCF-1 and OCF-5 are omitted for clarity. Red spheres stand for Ga, yellow for S, green for Zn, purple for Sn/Ga, orange for Se/S.

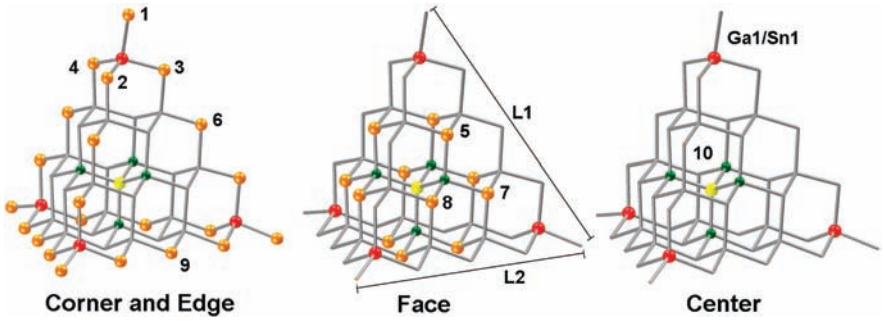

Figure 2. The labeling scheme for various Se^{2-} or S^{2-} sites in the T4 supertetrahedral cluster. The green spheres stand for Zn^{2+}, red for Ga^{3+}/Sn^{4+}, yellow for S^{2-}, orange for Se^{2-}/S^{2-}. L1 and L2 indicate the edge distance.

slightly doped T4-ZnGaSeS cluster in the same framework. The low doping level makes it difficult to determine the sulfur distribution in the T4 cluster through crystallographic refinement. Since we are interested in chemical and structural factors that control the maximum possible doping level, all reactions in this work use an excess amount of sulfur source (typically, the Se/DMSO molar ratio is approximately 1:10). In addition, the Sn/Zn molar ratio is limited to about 1 because our multiple experiments have shown that higher ratios led to the formation of UCR-20-Sn-Ga.[12a] Because of the heterogeneous nature of the reactants, a high temperature of 200 °C is employed.

Finally, the type of organic amines plays a key role in the final composition and topology of the framework. To examine effects of the amine-type on T4 clusters with different compositions (such as undoped T4-ZnGaSe, sulfur-doped T4-ZnGaSeS, tin-doped T4-ZnGaSnSe, and sulfur- and tin-doped T4-ZnGaSnSeS) and their assembly, a systematic study has been performed by using different amines (Scheme 2) with and without the addition of the sulfur and tin sources.

3.2. Cluster and Crystal Structures. In a typical undoped T4 $[Zn_4Ga_{16}Se_{35}]$ cluster, there are 18 bicoordinated Se^{2-} sites on six edges, 12 tricoordinated Se^{2-} ions on four faces, and one tetrahedral Se^{2-} at the core of T4, and the four terminal Se^{2-} ions. To satisfy Pauling's electrostatic valence rule, the core Se^{2-} site is surrounded by four zinc ions to give a bond valence sum of +2. All the structures in this work (OCF-1, OCF-5, and OCF-40) are based on this type of T4 cluster and topological types of OCF-1, OCF-5, and OCF-40 were previously reported.[12] OCF-40 is a molecular crystal consisting of isolated T4 clusters surrounded by protonated amine templates.[12e] However, both OCF-1 and OCF-5 have 3-D framework structures formed though corner-sharing T4 clusters, and they have different framework topologies, as shown in Figure 1.[12c] By treating each T4 cluster as a pseudotetrahedral atom, OCF-1 has the noninterpenetrating 3-D four-connected network, while OCF-5 has 2-fold interpenetrating diamond topology. Table 1 consists of a series of OCF-5 phases, each possessing some unique aspects, such as new amine type and cluster composition.

3.3. Site Selective Distribution of S and Sn in Zn−Ga−Se-based T4 Cluster. To conveniently describe the site-selective distribution of Se/S in the T4 cluster, all the Se^{2-} sites are labeled as shown in Figure 2. For doping by Sn, the situation is simpler, because both crystallographic refinements and consideration of bond valence indicate that dopant Sn^{4+} ions will occupy the corner metal sites. The refined occupancy factors for corner metal Sn/Ga and anionic Se/S sites are listed in Tables 2 and 3. As discussed below, the site-selective distribution of Se/S and Ga/Sn is dictated by chemical and structural factors. Samples synthesized from different batches show the consistent pattern of distribution within the experimental errors, as demonstrated by the analysis of three randomly selected crystals for both dual-doped OCF-5-ZnGaSnSeS-TMDP and OCF-5-ZnGaSnSeS-DAMP (Table 2). The reliability of occupancy refinement was supported by "control experiments" in which Se/S and Ga/Sn ratios are refined for samples made without Sn and/or S-doping. For example, for OCF-5-ZnGaSe-AEP obtained with neither Sn nor DMSO, the occupancy refinement gives the ratio of Sn/Ga close to 0:1 and the ratio of Se/S near 1:0.

In OCF-5-ZnGaSnSeS-TMDP with dual Sn- and S-doping, nearly 75% of Ga at the corner site is replaced by tin(IV). For anionic sites, sulfur doping occurs primarily at the core site (position 10, nearly 100% replacement) and at 12 face sites (positions 5, 7, 8, about 25%), while other sites remain relatively free from sulfur-doping. OCF-5-ZnGaSnSeS-ECHA has a similar doping pattern.

The doping pattern in dual-doped OCF-5-ZnGaSnSeS-DAMP is somewhat similar to that in OCF-5-ZnGaSnSeS-TMDP with two main differences: (1) a smaller degree of doping by Sn (about

dx.doi.org/10.1021/ja203143q | J. Am. Chem. Soc. 2011, 133, 9616–9625

Table 2. The Refined Occupancy Factors of Ga/Sn and Se/S in OCF-5-ZnGaSnSeS-TMDP and OCF-5-ZnGaSnSeS-DAMP at Various Crystallographic Sites with T4 Clusters

crystal		position occupancy between Se and S										
		Ga1/Sn1	Se1/S1	Se2/S2	Se3/S3	Se4/S4	Se5/S5	Se6/S6	Se7/S7	Se8/S8	Se9/S9	Se10/S10
TMDP	Batch 1	0.27108/0.72892	1.00021/-0.00013	0.93875/0.06124	0.90794/0.09205	0.96855/0.03144	0.80725/0.19276	0.95363/0.04636	0.73756/0.26244	0.70643/0.29358	0.97258/0.02743	0.00853/0.99144
	Batch 2	0.23172/0.76829	1.03378/-0.03377	0.93606/0.06394	0.90514/0.09485	0.95784/0.04215	0.81735/0.18267	0.95674/0.04327	0.74483/0.25517	0.71896/0.28104	0.95390/0.04610	0.00390/0.99609
	Batch 3	0.22650/0.77353	1.00027/ −0.00017	0.94810/0.05188	0.90033/0.09963	0.94828/0.05176	0.80801/0.19200	0.96635/0.03368	0.74684/0.25313	0.72822/0.27176	0.96760/0.03242	0.00078/0.99920
DAMP	Batch 1	0.46808/0.53192	1.01501/ −0.01501	0.90722/0.09278	0.87416/0.12583	0.93302/0.06699	0.77301/0.22700	0.96795/0.03206	0.74809/0.25191	0.72047/0.27953	0.96889/0.03111	0.00511/0.99488
	Batch 2	0.49967/0.50033	0.98540/0.01461	0.90224/0.09775	0.82651/0.17348	0.86948/0.13051	0.78870/0.21131	0.96103/0.03897	0.78580/0.21420	0.74828/0.25172	0.98617/0.01383	0.00584/0.99414
	Batch 3	0.47656/0.52343	1.01320/ −0.01318	0.89566/0.10431	0.86174/0.13824	0.91584/0.08414	0.77558/0.22443	0.97172/0.02831	0.75356/0.24643	0.73777/0.26222	0.97244/0.02756	0.00424/0.99574

Table 3. The Refined Occupancy Factors of Se/S and Ga/Sn in Select OCF-*n* at Various Crystallographic Sites with T4 Clusters

compounds	position occupancy between Se and S										
	Ga1/Sn1	Se1/S1	Se2/S2	Se3/S3	Se4/S4	Se5/S5	Se6/S6	Se7/S7	Se8/S8	Se9/S9	Se10/S10
OCF-5-ZnGaSe-AEP	0.97712/0.02279	1.00614/−0.00572	0.99829/0.00160	1.00173/−0.00159	0.97324/0.02659	0.96672/0.03341	1.00500/−0.00433	1.00049/−0.00061	1.00099/−0.00110	1.00095/−0.00095	0.96498/0.03502
OCF-5-ZnGaSnSe-2-MPR[12e]	0.53279/0.46701	1.00030/−0.00018	0.93759/0.06247	0.92535/0.07436	0.95530/0.04464	0.94763/0.05247	0.99973/0.00042	0.95552/0.04430	0.94978/0.05034	0.97590/0.02403	0.96790/0.03212
OCF-5-ZnGaSnSe-3-MPR[12e]	0.52924/0.47128	1.00017/−0.00010	0.93761/0.06237	0.92595/0.07407	0.95463/0.04530	0.94879/0.05132	0.99943/0.00053	0.95565/0.04436	0.94912/0.05082	0.97620/0.02382	0.96655/0.03335
OCF-5-ZnGaSeS-AEP	0.96331/0.03670	0.66814/0.33187	0.55827/0.44173	0.59762/0.40238	0.52932/0.47067	0.37655/0.62344	0.77252/0.22750	0.41888/0.58114	0.35519/0.64480	0.73872/0.26128	0.00484/0.99515
OCF-5-ZnGaSeS-DPM	0.99592/0.00415	0.81754/0.18249	0.69128/0.30865	0.67769/0.32226	0.72125/0.27869	0.46558/0.53454	0.85722/0.14272	0.48110/0.51889	0.43253/0.56743	0.86581/0.13420	0.00006/0.99985
OCF-5-ZnGaSnSeS-ECHA	0.26530/0.73467	0.99987/0.00014	0.91915/0.08080	0.89542/0.10457	0.93166/0.06824	0.81132/0.18871	0.98431/0.01578	0.76170/0.23807	0.74781/0.25189	1.00031/−0.00020	0.01811/0.98278
OCF-5-ZnGaSnSeS-PR	0.54242/0.45824	1.00118/−0.00093	0.89507/0.10475	0.88077/0.11895	0.91571/0.08423	0.73406/0.26554	0.99074/0.00926	0.75240/0.24707	0.71630/0.28333	0.96298/0.03717	0.03447/0.96554
OCF-40-ZnGaSnSeS-PR	0.50346/0.48654	0.91855/0.08146	0.97970/0.02027	0.97970/0.02027	0.97970/0.02027	0.89230/0.10777	0.88395/0.11605	0.89230/0.10777	0.89230/0.10777	0.88395/0.11605	0.26824/0.73178

dx.doi.org/10.1021/ja203143q | J. Am. Chem. Soc. 2011, 133, 9616–9625

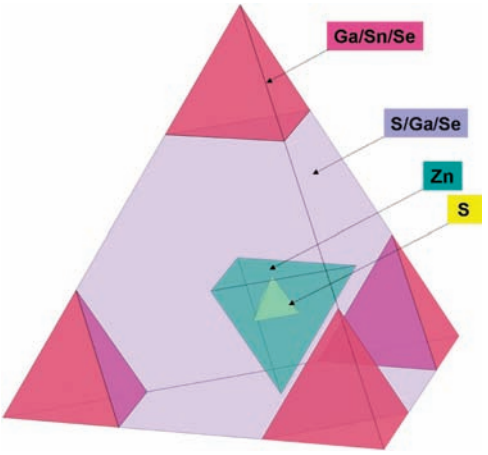

Figure 3. Illustration of selective elemental distribution in pentanary T4-ZnGaSnSeS cluster in OCF-5-ZnGaSnSeS-TMDP.

50% of Ga) at the corner site is observed; and (2) a greater degree of doping by sulfur at near-corner edge sites (positions 2, 3, 4). OCF-5-ZnGaSnSeS-PR has a doping pattern similar to OCF-5-ZnGaSnSeS-DAMP.

For sulfur-only doped OCF-5-ZnGaSeS-AEP and OCF-5-ZnGaSeS-DMP (no Sn at corner sites!), the core site (position 10) is also completely replaced by S^{2-}, as in Sn and S dual-doped samples. However, the sulfur-doping level at other positions is obviously different from that in dual-doped OCF-5-ZnGaSnSeS. The sulfur-doping level at face sites (positions 5, 7, 8) is greater than that in dual-doped OCF-5-ZnGaSnSeS-TMDP. Furthermore, even the corner (position 1) and edge sites (position 2, 3, 4, 6, 9) are partially doped by S^{2-}.

All the above observed doping behavior can be rationalized by a combination of Pauling's valence sum rule and Pearson's hard and soft acid base (HSAB) theory. First, the valence sum rule requires that four Zn^{2+} sites should surround the core Se^{2-} (or S^{2-} after doping) site at the center of T4 cluster and that high-valent Sn^{4+} sites should occupy the corner sites. Such a distribution of Zn^{2+} and Sn^{4+} then dictates the distribution of Se and S on the basis of HSAB theory. Sulfur prefers to occupy sites adjacent to Zn^{2+}, while selenium favors the sites closer to Sn^{4+} (Figure 3). In the undoped Zn−Ga−Se sample, the coordination environment of the core Se^{2-} site and 12 face sites are Zn_4Se and $ZnGa_2Se$, respectively. As a result, the core site Se^{2-} is most easily replaced by S^{2-}, while partial Se^{2-} replacement by S^{2-} occurs at face sites. It is particularly worth noting that the doping by Sn^{4+} suppresses the doping by sulfur. For example, in OCF-5-ZnGaSeS without Sn^{4+}, an average of approximately 50% of all Se sites is replaced by sulfur. In comparison, in Sn^{4+}-containing OCF-5-ZnGaSnSeS-TMDP, only an average of about 15% of Se sites are replaced by sulfur.

3.4. Effects of Amine-Type on Sn- and S-Doping and on Size and Charge of T4 Cluster. From the above, it is clear that the level of Sn^{4+}-doping, to a large degree, determines the level of S-doping in the Zn−Ga−Se system, in the reverse relationship. How is the level of Sn^{4+} doping controlled? The answer lies in the fundamental difference between Sn-doping and S-doping: the Sn-doping reduced the negative charge of the cluster while the S-doping has no effect on the charge of the cluster. Because Sn-doped clusters have a lower charge, it is therefore favored by organic amines with a low charge density based on the concept of

Table 4. Summary of M−Q (M = Zn, Ga, Sn; Q = S, Se) Bond Lengths

bond length (Å)	Zn	Ga	Sn
S	2.306−2.315	2.225−2.324	2.390−2.449
Se	2.399−2.438	2.369−2.424	2.421−2.562

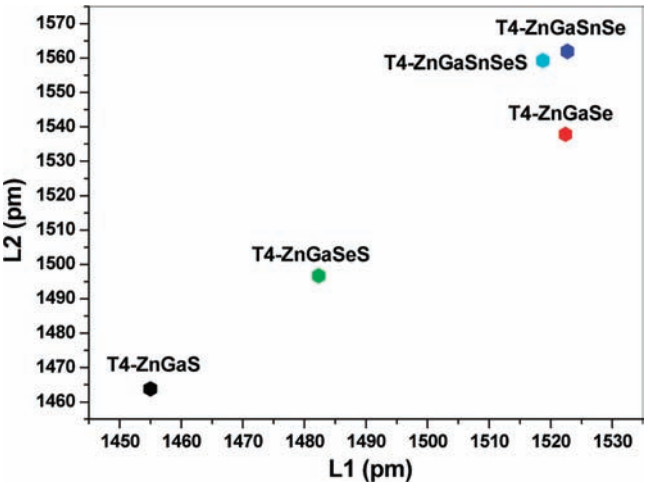

Figure 4. The size of five types of T4 cluster in OCF-5. The definition of L1 and L2 is shown in Figure 2.

the global (i.e., host−guest) charge-density matching. For this reason, protonated amine molecules such as TMDP (the C/N ratio 6.5) and ECHA (the C/N ratio 8) induce more tin doping at corner metal sites than DAMP (the C/N ratio 3) and PR (the C/N ratio 5) (The use of the C/N is only a rough estimate of the charge density of protonated amines; other factors such as molecular shape can also be relevant). In the present study, we have achieved two different ratios (i.e., 1:1 and 3:1) of Sn/Ga at corner sites, corresponding to $[Zn_4Ga_{14}Sn_2Se_{33}]^{8-}$ and $[Zn_4Ga_{13}Sn_3Se_{33}]^{7-}$, respectively. Thus, organic amines control the level of Sn-doping through host−guest charge density matching, which in turn controls the S-doping through the HSAB principle.

The Sn- and S-doping induce a systematic change in unit cell dimensions, as seen in OCF-5s (Table 1). In essence, it is the size of T4 clusters (and intercluster cavities) that is altered by doping (Figure 2). As expected from ionic radii (Se vs S, and Ga vs Sn) and related bond distances (Table 4), the size of the cluster increases with the doping level of Sn and decreases with the level of sulfur (Figure 4). Thus, T4-ZnGaSeS cluster is smaller than T4-ZnGaSe cluster, while T4-ZnGaSnSe cluster is larger than T4-ZnGaSe cluster. The dual-doping with Sn and S has two opposite effect on the cluster size. Thus, the size of T4-ZnGaSnSeS cluster lies between those of T4-ZnGaSnSe and T4-ZnGaSeS clusters. It is worth emphasizing that a minor change in the dimension of clusters is sometimes essential for achieving host−guest charge-density matching needed for crystallization and can also lead to a different framework topology, as discussed below.

3.5. Phase Selectivity Controlled by Amine Type and Doping. Because amine-type and doping by Sn and S can be individually changed when preparing reaction mixtures, it is possible to achieve synthetic controls using any of these three factors. Scheme 3 summarizes the effects of Sn- and S-doping when four different types of amines are used. ECHA and DAMP

Scheme 3. Schematic of Reactions in Presence of Different Amine Templates and Auxiliary Reactants[a]

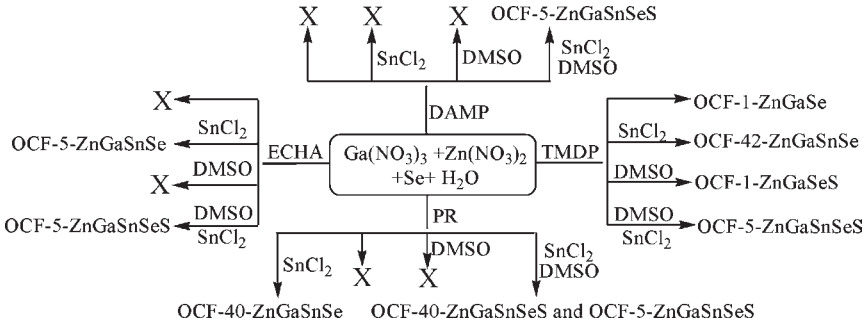

[a] X means no crystalline products are obtained.

represent the simplest case, as both give OCF-5 only. The difference is that DAMP gives OCF-5-ZnGaSnSeS-DAMP only through dual Sn- and S-dopings where ECHA can form OCF-5 with either single Sn-doping or with dual doping. Other reaction conditions (e.g., no doping, or no Sn-doping) results in no crystallization. Thus, for both ECHA and DAMP, the incorporation of Sn is essential for crystallization.

Piperidine (PR) is similar to DAMP and ECHA, in a sense that Sn is required for crystallization. However, the product is quite different and involves two different phases (OCF-40 and OCF-5). With no or small amount of DMSO, OCF-40-ZnGaSnSe is the only product. However, as more DMSO is added, a mixture of OCF-40-ZnGaSnSeS-PR (minor phase) and OCF-5-ZnGaSnSeS-PR (major phase) is obtained.

TMDP is more versatile and can generate three different phases (OCF-1, OCF-5, and OCF-42) (Scheme 3). As long as Sn is absent, the product is OCF-1-ZnGaSe-TMDP (without Sn, DMSO causes S-doping in OCF-1, but does not affect the framework topology). When only Sn (no DMSO) is added, a totally different structure containing both T2 and T4 clusters, OCF-42-ZnGaSnSe-TMDP, is formed.[12d] Finally, like other three amines, OCF-5-ZnGaSnSeS-TMDP is formed with dual-doping.

The correlation between the doping strategy and the structure type can be summarized as the following. In the absence of any doping or with only S-doping, OCF-1 is obtained with TMDP (no crystallization with other amines). With both Sn- and S-doping, OCF-5 is obtained (for all four amine types). The most sensitive phase selectivity by amines come when only Sn-doping is used, resulting in three different phases, OCF-5 (for ECHA), OCF-40 (for PR),[12e] and OCF-42 (for TMDP).[12d]

3.6. Effects of Cluster Size and Charge on the Phase Selectivity. The above observed phase selectivity reveals important factors that control the crystallization of chalcogenide clusters. For a particular phase to crystallize, organic amine molecules need to possess proper charge, size, and shape for matching with the charge of the cluster and size of the intercluster cavity, which is dependent on the Sn- and S-doping. Given a particular amine, the synthetic system endowed with more ways to tune its framework charge density is more likely to find a way to crystallize, which is easily proved by Scheme 3.

Scheme 3 shows a total of 16 synthetic paths. With no doping and minimum flexibility in charge density tuning, only 1 out 4 paths leads to crystallization. The S-doping only slightly reduces the cluster size, but does not alter the charge of the cluster. It is not surprising that only 1 out 4 paths leads to crystallization. The Sn-only doping provides the flexibility to alter both charge and size of the cluster, which provides a greater freedom in the charge density tuning. As a result, 3 out 4 paths lead to crystallization. The greatest flexibility comes from the combined S- and Sn-doping, which leads the crystallization in 4 out of 4 paths.

It is worth noting that while the size reduction caused by S-doping is in itself not adequate for the phase selectivity, it does exhibit a controlling effect when used in combination with Sn-doping. For example, Sn-only doped OCF-5-ZnGaSnSe-TMDP cannot be made, possibly because protonated TMDP does not match with $[Zn_4Ga_{13}Sn_3Se_{33}]^{7-}$ to generate OCF-5-ZnGaSnSe-TMDP. However, TMDP does match the S- and Sn-dual-doped size-shrunken $[Zn_4Ga_{13}Sn_3Se_{33-x}S_x]^{7-}$ T4 cluster to form OCF-5-ZnGaSnSeS-TMDP. The same is true for OCF-5-ZnGaSnSeS-DAMP and OCF-5-ZnGaSnSeS-PR both of which require dual S- and Sn-doping.

OCF-42-ZnGaSnSe, made by TMDP and the only Sn-doping, reveals another way to realize the global charge density matching. It is composed of Sn-doped $[Sn_{1.6}Ga_{2.4}Se_8]$ T2 cluster and undoped $[Zn_4Ga_{16}Se_{33}]^{10-}$ T4 cluster, instead of Sn-doped T4 $[Zn_4Ga_{13}Sn_3Se_{33}]^{7-}$ cluster seen in OCF-5. Why is not T4 cluster doped with Sn? Clearly, the charge of Sn-doped $[Zn_4Ga_{13}Sn_3Se_{33}]^{7-}$ T4 cluster in combination with T2 cluster does not match with protonated TMDP, which only matches the more negative $[Zn_4Ga_{16}Se_{33}]^{10-}$ T4 cluster and T2 clusters to form OCF-42-ZnGaSnSe-TMDP.

The synthesis of OCF-40 using piperidine has an unusual feature not found in other amine-templated systems. This feature is that OCF-40 can accept a very limited amount of the S-doping and an increased amount of DMSO shifts the phase selection from OCF-40 to OCF-5. OCF-40-ZnGaSnSe-PR is composed of isolated Sn-doped $[Zn_4Ga_{14}Sn_2Se_{35}]^{12-}$ cluster and piperidinium. Twenty-four piperidinium ions compactly cover the surface the T4 cluster by Se···H—N hydrogen bonds. In this case, the charge balance and size match between the cluster and 24 amine cations are critical to the formation of OCF-40-ZnGaSnSe-PR. In fact, it has been found that the substituted piperidine (such as 2-MPR, 3-MPR, and 2,2,6,6-TMPR) tend to give OCF-5-ZnGaSnSe, which is because the Sn-doped $[Zn_4Ga_{14}Sn_2Se_{35}]^{12-}$ T4 cluster does not have enough surface area to accommodate these more bulky amines to form OCF-40-ZnGaSnSe.

While the Sn-doped T4 $[Zn_4Ga_{14}Sn_2Se_{35}]^{12-}$ cluster in OCF-40 cannot generally accommodate amine molecules other than piperidine, it does allow a limited amount of S-doping to give

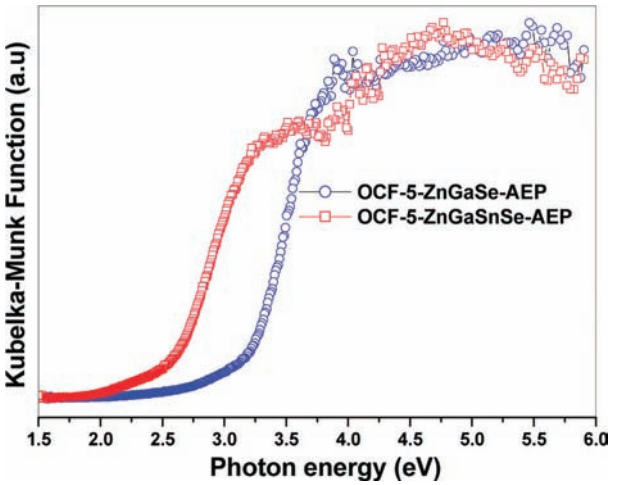

Figure 5. Normalized solid-state UV−vis adsorption spectra of OCF-5-ZnGaSe-AEP and OCF-5-ZnGaSnSe-AEP, showing the red shift caused by Sn-doping.

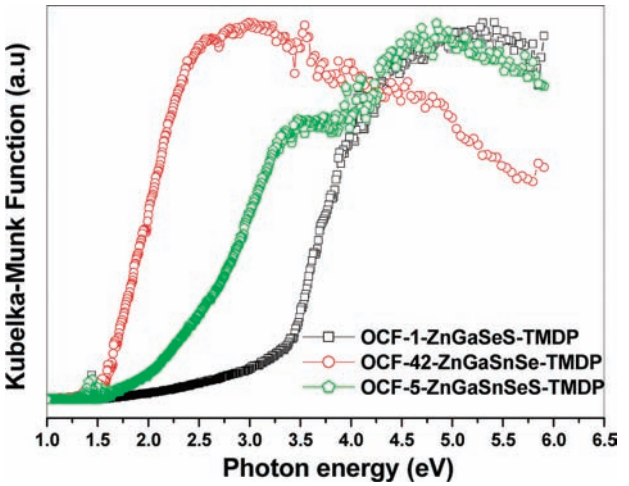

Figure 6. Normalized solid-state UV−vis adsorption spectra of OCF-1-ZnGaSeS-TMDP, OCF-5-ZnGaSnSeS-TMDP, and OCF-42-ZnGaSnSe-TMDP.

somewhat smaller Sn- and S-dual doped $[Zn_4Ga_{14}Sn_2Se_{35-x}S_x]^{12-}$ T4 cluster. However, the level of S-doping in OCF-40-ZnGaSnSeS-PR, as evidenced by the sulfur occupancy factor at both core site and face sites, is much lower than that in OCF-5-ZnGaSnSeS-PR. This means that the core site in OCF-40 cannot be completely occupied by S^{2-}. As a matter of fact, OCF-40-ZnGaSnSeS-PR is the "co-crystal" of Sn-doped $[Zn_4Ga_{14}Sn_2Se_{35}]^{12-}$ T4 cluster and dual-doped $[Zn_4Ga_{14}Sn_2Se_{35-x}S_x]^{12-}$ T4 cluster. With an increased amount of $[Zn_4Ga_{14}Sn_2Se_{35-x}S_x]^{12-}$ clusters, OCF-5-ZnGaSnSeS-PR becomes the preferred framework for better matching with the protonated piperidine.

3.7. Optical Properties. Since optical properties (such as electronic band gaps) of solid-state semiconductors are strongly influenced by chemical compositions and crystal structures, the ability to create these multicomponent chalcogenides with different structures makes it possible to achieve a wide range of band structures in these materials. In this work, the fact that Sn-doping causes a red shift while S-doping causes a blue shift (Figures 5−8) greatly boosts the range of band gaps that can be achieved (e.g., 1.54 eV for Sn-doped OCF-42-ZnGaSnSe-TMDP and 3.37 eV for S-doped OCF-1-ZnGaSeS-TMDP).

The synthesis of a series of framework materials (e.g., OCF-5 series) with the same framework topology, but different framework compositions provides an excellent opportunity for probing effects of chemical compositions on band structures, without the complications caused by the variation in framework topologies. As shown by Figure 5, the Sn-doping into the gallium leads to a red shift in the band gap, as demonstrated by undoped OCF-5-ZnGaSe-AEP (band gap, 3.23 eV) and Sn-doped OCF-5-ZnGaSnSe-AEP (band gap, 2.49 eV). On the other hand, S-doping causes a blue shift in the band gap, as evidenced by undoped OCF-1-ZnGaSe-TMDP (band gap, 1.71 eV) and S-doped OCF-1-ZnGaSeS-TMDP (band gap, 3.37 eV) (Figure 6). The similar S-doping effect is also observed in Sn-doped OCF-5-ZnGaSnSe-ECHA (band gap, 2.24 eV) and dual-doped OCF-5-ZnGaSnSeS-ECHA (band gap, 2.54 eV) (Figure 7).

Because Sn-doping and S-doping have opposite effects on the band gaps, the dual-doped sample is expected to have a band gap between Sn-doped and S-doped phases. However, a complication occurs when comparing the undoped sample and the

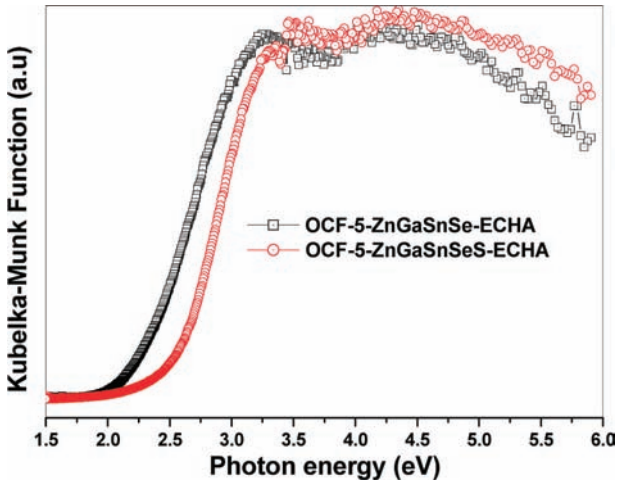

Figure 7. Normalized solid-state UV−vis adsorption spectra of OCF-5-ZnGaSnSe-ECHA and OCF-5-ZnGaSnSeS-ECHA, showing the blue shift caused by S-doping.

dual-doped sample, in which case the direction of the shift by the dual-doped sample would depend on which dopant (Sn or S) plays a dominant role. A comparison between undoped OCF-5-ZnGaSe-AEP (band gap, 3.23 eV) and dual-doped OCF-5-ZnGaSnSeS-ECHA (band gap, 2.54 eV) seems to suggest that Sn has a stronger effect than S (if the difference in the amine-type is not taken into consideration). Note that it is possible that the S-doping can cause a more dramatic shift than the Sn-doping, when each dopant is applied individually (i.e., when comparing S-doped sample with Sn-doped sample). However, in the case of dual doping by both Sn and S, the level of S-doping is suppressed (as discussed above based on the HSAB principle) by the Sn-doping, which may lead to the greater control of the band gap by Sn rather than S, as shown in Scheme 4.

In addition to Sn- and S-doping, the nature of organic amines also affects the electronic properties. Organic amines can affect not only the topological types, but also the level of doping and

dx.doi.org/10.1021/ja203143q |J. Am. Chem. Soc. 2011, 133, 9616–9625

Scheme 4. Possible Band Gap on Selenide Superlattices Composed of Four Different Clusters

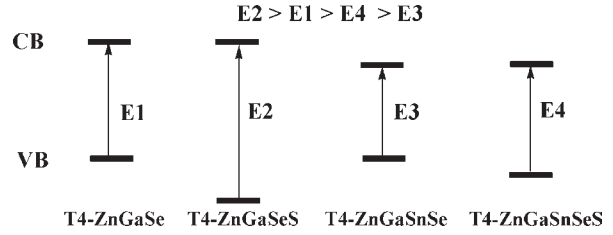

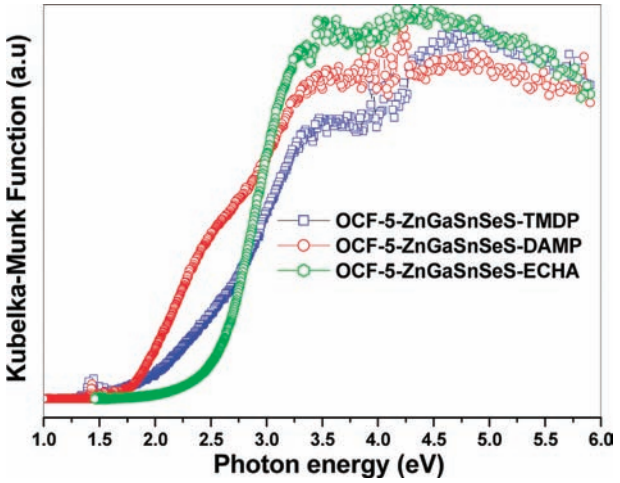

Figure 8. Normalized solid-state UV−vis adsorption spectra of OCF-5-ZnGaSnSeS-TMDP, OCF-5-ZnGaSnSeS-DAMP, and OCF-5-ZnGaSnSeS-ECHA.

distribution of dopant in different sites. Still, given the same framework structure, effects of organic amines on band structures appear to be smaller than Sn- and/or S-doping, as seen for OCF-5-ZnGaSnSeS-TMDP, OCF-5-ZnGaSnSeS-DAMP, and OCF-5-ZnGaSnSeS-ECHA (Figure 8).

4. CONCLUSIONS

We have synthesized a series of Sn- and/or S-doped open-framework covalent selenide superlattices and isolated nanoscale molecules, all of which are composed of multicomponent super-tetrahedral T4 cluster and protonated amine templates. It is discovered that Sn- and S-doping has a dramatic effect on the crystallization of Zn−Ga−Se clusters and frameworks, because of the extraordinarily high sensitivity of the framework formation process to the charge and size of both organic templates and the size and charge of the T4 clusters, the latter of which can be fine-tuned by Sn- and S-doping. It is demonstrated that a chemical system with the greatest flexibility in self-adjusting the cluster size and pore dimension (e.g., through the presence of metal ions such as $Sn^{4+}/Ga^{3+}/Zn^{2+}$ with comparable bonding geometry, but complementary oxidation states) is the easiest to form a crystalline framework capable of accommodating different types of template amine molecules being employed. Amines with low charge density encourage a higher level of Sn-doping because the replacement of Ga^{3+} by Sn^{4+} serves to reduce the negative charge of the cluster and framework. A high level of S-doping (up to 100% at certain sites) is possible. Yet, when co-doped with Sn^{4+}, the doping level of S can be suppressed by the Sn-doping because of the Sn's stronger affinity for Se. The highly site selective distribution of Sn within the T4 clusters is controlled by the valence sum rule while the site selective distribution of S within the T4 cluster is largely controlled by sulfur's affinity for Zn. The availability of a diversity of compositions and structures has made it possible to tune the electronic band gap over a large range from about 1.5 to 3.4 eV.

■ ASSOCIATED CONTENT

Supporting Information. Additional figures and CIF files. This material is available free of charge via the Internet at http://pubs.acs.org.

■ AUTHOR INFORMATION

Corresponding Author
pingyun.feng@ucr.edu

■ ACKNOWLEDGMENT

We thank the support of this work by NSF (P.F.; CHEM-0809335) and NSF (X.B.; DMR-0846958). P.F. is a Camille Dreyfus Teacher Scholar and X.B. is a Henry Dreyfus Teacher Scholar.

■ REFERENCES

(1) (a) Kobayakawa, K.; Teranishi, A.; Tsurumaki, T.; Sato, Y.; Fujishima, A. *Electrochim. Acta* **1992**, *37*, 465–467. (b) Lei, Z; You, W.; Liu, M.; Zhou, G.; Takata, T.; Hara, M.; Domen, K.; Li, C. *Chem. Commun.* **2003**, *17*, 2142–2143. (c) Chen, D.; Ye, J. H. *J. Phys. Chem. Solids* **2007**, *68*, 2317–2320.

(2) (a) Kanatzidis, M. G.; Huang, S. P. *Inorg. Chem.* **1989**, *28*, 4667–4669. (b) Mrotzek, A.; Kanatzidis, M. G. *Acc. Chem. Res.* **2003**, *36*, 111–119. (c) Hsu, K. F.; Loo, S.; Guo, F.; Chen, W.; Dyck, J. S.; Uher, C.; Hogan, T.; Polychroniadis, E. K.; Kanatzidis, M. G. *Science* **2004**, *303*, 818–821. (d) Arachchige, I. U.; Wu, J.; Dravid, V. P.; Kanatzidis, M. G. *Adv. Mater.* **2008**, *20*, 3638–3642. (e) Cook, B. A.; Kramer, M. J.; Harringa, J. L.; Han, M. K.; Chung, D. Y.; Kanatzidis, M. G. *Adv. Funct. Mater.* **2009**, *19*, 1254–1259.

(3) (a) Mohanan, J. L.; Brock, S. L. *J. Non-Cryst. Solids* **2004**, *350*, 1–8. (b) Mohanan, J. L.; Arachchige, I. U.; Brock, S. L. *Science* **2005**, *307*, 397–401. (c) Mohanan, J. L.; Brock, S. L. *J. Sol.-Gel Sci. Technol.* **2006**, *40*, 341–350. (d) Brock, S. L.; Arachchige, I. U.; Kalebaila., K. K. *Comments Inorg. Chem.* **2006**, *27*, 103–126. (e) Yu, H.; Brock, S. L. *ACS Nano* **2008**, *2*, 1563–1570. (f) Yao, Q.; Arachchige, I. U.; Brock, S. L. *J. Am. Chem. Soc.* **2009**, *131*, 2800–2801. (g) Yao, Q.; Brock, S. L. *Nanotechnology* **2010**, *21*, 115502/1–115502/10. (h) Pawsey, S.; Kalebaila, K. K.; Moudrakovski, I.; Ripmeester, J. A.; Brock, S. L. *J. Phys. Chem. C* **2010**, *114*, 131871–3195.

(4) (a) Zheng, N.; Bu, X.; Feng, P. *Nature* **2003**, *426*, 428–432. (b) Zheng, N.; Bu, X.; Vu, H.; Feng, P. *Angew. Chem., Int. Ed.* **2005**, *44*, 5299–5303.

(5) (a) Zimmerman, C.; Melullis, M.; Dehnen, S. *Angew. Chem., Int. Ed.* **2002**, *41*, 4269–4271. (b) Dehnen, S.; Brandmayer, M. K. *J. Am. Chem. Soc.* **2003**, *125*, 6618–6619. (c) Zimmermann, C.; Anson, C. E.; Weigend, F.; Clérac, R; Dehnen, S. *Inorg. Chem.* **2005**, *44*, 5686–5695. (d) Dehnen, S.; Melullis, M. *Coord. Chem. Rev.* **2007**, *251*, 1259–1280.

(6) (a) Parise, J. B.; Tan, K. *Chem. Commun.* **1996**, 1687–1688. (b) Cahill, C. L.; Parise, J. B. *Chem. Mater.* **1997**, *9*, 807–811. (c) Cahill, C. L.; Ko, Y.; Parise, J. B. *Chem. Mater.* **1998**, *10*, 19–21. (d) Cahill, C. L.; Parise, J. B. *J. Chem. Soc., Dalton Trans.* **2000**, 1475–1482.

(7) (a) Lee, G. S. H.; Craig, D. C.; Ma, I.; Scudder, M. L.; Bailey, T. D.; Dance, I. G. *J. Am. Chem. Soc.* **1988**, *110*, 4863–4864. (b) Dance, I. G.; Fisher, K. G. *Prog. Inorg. Chem.* **1994**, *41*, 637–803. (c) Fenske, D.; Zhu, N.; Langetepe, T. *Angew. Chem., Int. Ed.* **1998**, *37*, 2640–2644. (d) Soloviev, V. N.; Eichhofer, A.; Fenske, D.; Banin, U. *J. Am. Chem. Soc.* **2001**, *123*, 2354–2364. (e) Dehnen, S.; EichhOfer, A.; Fenske, D. *Eur. J. Inorg. Chem.* **2002**, *2*, 279–317. (f) Corrigan, J. F.; Fuhr, O.; Fenske, D. *Adv. Mater.* **2009**, *21*, 1867–1871.

(8) (a) Yaghi, O. M.; Sun, Z.; Richardson, D. A.; Groy, T. L. *J. Am. Chem. Soc.* **1994**, *116*, 807–808. (b) Li, H.; Laine, A.; O'Keeffe, M.; Yaghi, O. M. *Science* **1999**, *283*, 1145–1147. (c) Li, H.; Eddaoudi, M.; Laine, A.; O'Keeffe, M.; Yaghi, O. M. *J. Am. Chem. Soc.* **1999**, *121*, 6096–6097. (d) Li, H.; Kim, J.; Groy, T. L.; O'Keeffe, M.; Yaghi, O. M. *J. Am. Chem. Soc.* **2001**, *123*, 4867–4868. (e) Li, H.; Kim, J.; O'Keeffe, M.; Yaghi, O. M. *Angew. Chem., Int. Ed.* **2003**, *42*, 1819–1821.

(9) (a) Vaqueiro, P.; Romero, M. L. *J. Phys. Chem. Solids* **2007**, *68*, 1239–1243. (b) Vaqueiro, P.; Romero, M. L. *Chem. Commun.* **2007**, 3282–3284. (c) Vaqueiro, P.; Romero, M. L. *J. Am. Chem. Soc.* **2008**, *130*, 9630–9631. (d) Vaqueiro, P.; Romero, M. L.; Rowan, B. C.; Richards, B. S. *Chem.—Eur. J.* **2010**, *16*, 4462–4465.

(10) Su, W.; Huang, X.; Li, J.; Fu, H. *J. Am. Chem. Soc.* **2002**, *124*, 12944–12945.

(11) (a) Wang, C.; Li, Y.; Bu, X.; Zheng, N.; Zivkovic, O.; Yang, C. S.; Feng, P. *J. Am. Chem. Soc.* **2001**, *123*, 11506–1507. (b) Bu, X.; Zheng, N.; Li, Y.; Feng, P. *J. Am. Chem. Soc.* **2002**, *124*, 12646–12647. (c) Wang, C.; Bu, X.; Zheng, N.; Feng, P. *Angew. Chem., Int. Ed.* **2002**, *41*, 1959–1961. (d) Zheng, N.; Bu, X.; Feng, P. *J. Am. Chem. Soc.* **2003**, *125*, 1138–1139. (e) Bu, X.; Zheng, N.; Li, Y.; Feng, P. *J. Am. Chem. Soc.* **2003**, *125*, 6024–6025. (f) Zheng, N.; Bu, X.; Feng, P. *Angew. Chem., Int. Ed.* **2004**, *43*, 4753–4755. (g) Bu, X.; Zheng, N.; Feng, P. *Chem.—Eur. J.* **2004**, *10*, 3356–3362. (h) Feng, P.; Bu, X.; Zheng, N. *Acc. Chem. Res.* **2005**, *38*, 293–303. (i) Zhang, Q.; Bu, X.; Zhang, J.; Wu, T.; Feng, P. *J. Am. Chem. Soc.* **2007**, *129*, 8412–8413. (j) Zhang, Z.; Zhang, J.; Wu, T.; Bu, X.; Feng, P. *J. Am. Chem. Soc.* **2008**, *130*, 15238–15239. (k) Wang, L.; Wu, T.; Zuo, F.; Zhao, X.; Bu, X.; Wu, J.; Feng, P. *J. Am. Chem. Soc.* **2010**, *132*, 3283–3285.

(12) (a) Zheng, N.; Bu, X.; Wang, B.; Feng, P. *Science* **2002**, *298*, 2366–2369. (b) Wang, C.; Bu, X.; Zheng, N.; Feng, P. *Chem. Commun.* **2002**, 1344–1345. (c) Bu, X.; Zheng, N.; Wang, X.; Wang, B.; Feng, P. *Angew. Chem., Int. Ed.* **2004**, *43*, 1502–1505. (d) Wu, T.; Wang, X.; Bu, X.; Zhao, X.; Wang, L.; Feng, P. *Angew. Chem., Int. Ed.* **2009**, *44*, 7340–7343. (e) Wu, T.; Wang, L.; Bu, X.; Chau, V.; Feng, P. *J. Am. Chem. Soc.* **2010**, *132*, 10823–10831.

(13) (a) Ding, N.; Chung, D. Y.; Kanatzidis, M. G. *Chem. Commun.* **2004**, 1170–1171. (b) Manos, M. J.; Iyer, R. G.; Quarez, E.; Liao, J. H.; Kanatzidis, M. G. *Angew. Chem., Int. Ed.* **2005**, *44*, 3552–3555. (c) Tsamourtzi, K.; Song, J. H.; Bakas, T.; Freeman, A. J.; Trikalitis, P. N.; Kanatzidis, M. G. *Inorg. Chem.* **2008**, *47*, 11920–11929. (d) Manos, M. J.; Chrissafis, K.; Kanatzidis, M. G. *J. Am. Chem. Soc.* **2006**, *128*, 8875–8883.

(14) (a) DeGroot, M. W.; Rösner, H.; Corrigan, J. F. *Chem.—Eur. J.* **2006**, *12*, 1547–1554. (b) Pradhan, N.; Goorskey, D.; Thessing, J.; Peng, X. *J. Am. Chem. Soc.* **2005**, *127*, 17586–17587. (c) Pradhan, N.; Peng, X. *J. Am. Chem. Soc.* **2007**, *129*, 3339–3347. (d) Deng, Z. T.; Yan, H.; Liu, Y. *J. Am. Chem. Soc.* **2009**, *131*, 17744–17745. (e) Srivastava, B. B.; Jana, S.; Pradhan, N. *J. Am. Chem. Soc.* **2011**, *133*, 1007–1015.

(15) (a) Rothenberger, A.; Morris, C.; Wang, H. H.; Chung, D. Y.; Kanatzidis, M. G. *Inor. Chem.* **2009**, *48*, 9036–9040. (b) Manos, M. J.; Kanatzidis, M. G. *J. Am. Chem. Soc.* **2009**, *131*, 6599–6607.

(16) (a) Lips, F.; Dehnen, S. *Inorg. Chem.* **2008**, *47*, 5561–5563. (b) Ruzin, E.; Zent, E.; Matern, E.; Massa, W.; Dehnen, S. *Chem.—Eur. J.* **2009**, *15*, 5230–5244.